American Mineralogist, Volume 82, pages 51–60, 1997

Structure and elasticity of MgO at high pressure

B.B. KARKI,[1] L. STIXRUDE,[2] S.J. CLARK,[1] M.C. WARREN,[1]
G.J. ACKLAND,[1] AND J. CRAIN[1]

[1]Department of Physics and Astronomy, University of Edinburgh, Edinburgh, EH9 3JZ Scotland, U.K.
[2]School of Earth and Atmospheric Sciences, Georgia Institute of Technology, Atlanta, Georgia 30332-0340, U.S.A.

ABSTRACT

The structural and elastic properties of MgO periclase were studied up to 150 GPa with the first-principles pseudopotential method within the local density approximation. The calculated lattice constant of the B1 phase over the pressure range studied is within 1% of experimental values. The observed B1 phase of MgO was found to be stable up to 450 GPa, precluding the B1-B2 phase transition within the lower mantle. The calculated transition pressure is less than one-half of the previous pseudopotential prediction but is very close to the linearized augmented plane-wave result. All three independent elastic constants, c_{11}, c_{12}, and c_{44}, for the B1 phase are calculated from direct computation of stresses generated by small strains. The calculated zero-pressure values of the elastic moduli and wave velocities and their initial pressure dependence are in excellent agreement with experiments. MgO was found to be highly anisotropic in its elastic properties, with the magnitude of the anisotropy first decreasing between 0 and 15 GPa and then increasing from 15 to 150 GPa. Longitudinal and shear-wave velocities were found to vary by 23 and 59%, respectively, with propagation direction at 150 GPa. The character of the anisotropy changes qualitatively with pressure. At zero pressure longitudinal and shear-wave propagations are fastest along [111] and [100], respectively, whereas above 15 GPa, the corresponding fast directions are [100] and [110]. The Cauchy condition was found to be strongly violated in MgO, reflecting the importance of noncentral many-body forces.

INTRODUCTION

The elasticity of minerals at high pressure is of substantial physical and geological interest for several reasons. First, our most precise and informative observations of the bulk of the Earth are from its elastic properties. Comparisons between seismological observations and the elastic properties of candidate mantle minerals and assemblages are the only way to extract information regarding the composition and mineralogy of the mantle from the rich seismological database. Second, the geometry of mantle flow can be illuminated by comparing seismological observations of mantle anisotropy with the measured or predicted anisotropy of hypothesized mantle phases. Finally, the elasticity of minerals yields substantial insight into the nature of bonding. For example, deviations from the Cauchy relations are a direct measure of the importance of noncentral forces in crystals. As the end-member of a hypothesized major lower mantle phase, (Mg,Fe)O magnesiowüstite, the elasticity of periclase is particularly relevant in this context. The exceptionally wide stability field of this mineral (>200 GPa) makes studies of its elasticity an ideal testing ground for our understanding of the effect of pressure on elasticity. Moreover, our predictions of the elasticity of periclase over a wide range of pressure provide a test of the predictive ability of first-principles theoretical methods.

Both diamond-cell (Duffy et al. 1995) and shock-wave (Vassiliou and Ahrens 1981) measurements have found the observed B1 structure of MgO to be stable up to at least 227 and 200 GPa, respectively, indicating the absence of the usual B1(NaCl)-B2(CsCl) structural phase transition of alkaline-earth oxides in MgO. These data are consistent with the results of theoretical calculations based on first-principles pseudopotential (Chang and Cohen 1984), linearized augmented plane-wave (Mehl and Cohen 1988), ab initio potential-induced-breathing (PIB) (Isaak et al. 1990), and modified PIB models (Zhang and Bukowinski 1991), which have predicted 1050, 510, 486, and 580 GPa, respectively, for the B1-B2 phase transition in MgO, well above the pressure of the core-mantle boundary. In contrast to the equation of state, the study of the high-pressure elastic behavior of MgO is limited both experimentally and theoretically. Although the temperature dependence of elastic properties has been studied over a wide range of temperatures at ambient pressure by resonance methods (Isaak et al. 1989), experimental studies of the effect of pressure are confined to pressures <3 GPa (Bogardus 1965; Anderson and Andreatch 1966; Chang and Barsch 1969; Spetzler 1970; Jackson and Niesler 1982). There have been no first-principles predictions of the elastic moduli of this mineral, although Isaak et al. (1990) performed a detailed study of it elasticity on

0003–004X/97/0102–0051$05.00

the basis of the PIB model, and Inbar and Cohen (1995) studied its thermoelastic properties according to PIB.

Here we present a first-principles study of the structure and elasticity of MgO at lower mantle pressures (zero temperature) with use of the total-energy pseudopotential method. We obtained the equation of state for the B1 structure of MgO up to 150 GPa, which exceeds the highest value reached in the lower mantle. We also calculated the B1-B2 phase-transition pressure by comparing the enthalpy of the two phases of MgO at different pressures. By computing the stresses generated by small deformations of the equilibrium primitive cell, we determined all three elastic constants, c_{11}, c_{12}, and c_{44}, which were then used to calculate the bulk and shear moduli and hence the isotropic longitudinal and shear velocities as a function of pressure. We also calculated the wave velocities in different crystallographic directions to study the elastic anisotropy of MgO. Finally, we studied the violation of the Cauchy condition in MgO.

Methods

Structural optimization

The computations are based on density functional theory, which is, in principle, an exact theory of the ground state (Kohn and Sham 1965). Two approximations were made. First, we used the local density approximation (LDA) to the exchange-correlation energy functional. The LDA has been widely studied in applications involving essentially all classes of materials, including oxides (Mehl and Cohen 1988). Second, the underlying idea of the pseudopotential approximation is to recognize that the core electrons are essentially static (frozen) and do not vary their charge density significantly under perturbations to the lattice. The pseudopotential mimics the potential seen by the valence electrons because of the nucleus and frozen core electrons. This approximation has been studied in a wide variety of insulating and semiconducting systems (Wentzcovitch et al. 1995; Cohen and Chelikowsky 1988).

We simulated a two-ion primitive cell of MgO by using the first-principles pseudopotential method (Payne et al. 1992). The optimized, norm-conserving, nonlocal pseudopotentials generated by the Q_c tuning method (Lee 1995; Lin et al. 1993) were used in the Kleinman-Bylander form (Kleinman and Bylander 1982). The reference atomic configurations used to construct the O pseudopotential (p local) were $2s^2 2p^4$ for the s and p components and $2s^1 2p^{1.75} 3d^{0.25}$ for the d component, with real-space core radius r_c(s,p,d) = 1.4 a.u. and $Q_c/\mathbf{q}_3$(s,p,d) = (0.40,1.11,1.0325). Here, Q_c is the control parameter connected with the kinetic energy of the pseudo wave function to tune the pseudopotential, and $\mathbf{q}_3$ is the largest wave vector in the Fourier expansion (in terms of spherical Bessel functions) of the pseudo wave function. For the magnesium pseudopotential, the s component (local) was constructed with reference atomic configuration of $3s^2$, r_c(s) = 2.0 a.u. and $Q_c/\mathbf{q}_3$(s) = 1.0. Both pseudopotentials have been shown to be highly transferable by using them in structural and elasticity calculations of $MgSiO_3$ perovskite and SiO_2 (Karki et al., in preparation). The parameterization of Perdew and Zunger (1981) was used for the exchange-correlation potential in LDA. The valence electronic wave functions were expanded in a plane-wave basis set truncated at a maximum plane-wave energy (the cutoff energy) of 900 eV. This cutoff energy yielded 1200 basis functions per band. The Brillouin zone was sampled on a 4 × 4 × 4 Monkhurst-Pack (Monkhurst and Pack 1976) special k mesh yielding ten k points in the irreducible wedge. Careful convergence tests showed that increasing the cutoff energy to 1500 eV lowered the total energy by only 0.047 eV, whereas increasing the number of the special k points from two (2 × 2 × 2 k-point mesh) to ten raised the total energy by only 0.012 eV. Thus, the estimated numerical precision in our calculated total energies is within 0.06 eV at all volumes.

The self-consistent total energies and Hellman-Feynman forces were found by solving the Kohn-Sham equations with use of a preconditioned conjugate-gradient method. The periclase structure was optimized for a series of applied pressures by minimizing the self-consistent Hellman-Feynman forces and stresses. Efficient minimization was achieved by employing a generalized dynamics that is governed by the Lagrangian (Wentzcovitch 1991; Wentzcovitch et al. 1993; Hsueh et al. 1996; Warren and Ackland 1996)

$$L = \sum_{i=1}^{N} \frac{m_i}{2} \dot{\mathbf{s}}_i^T \mathbf{g} \dot{\mathbf{s}}_i + \frac{W}{2} Tr(\dot{\mathbf{h}} \mathbf{f}_0 \dot{\mathbf{h}}^T) - E(\mathbf{r}_i) - PV \quad (1)$$

where W is the fictitious boxmass, $\mathbf{g} = \mathbf{h}^T\mathbf{h}$ is the metric tensor, with $\mathbf{h}$ defined from the unit-cell vectors such that rescaled ionic coordinates are $\mathbf{r}_i = \mathbf{h}\mathbf{s}_i$, and similarly $\mathbf{f}_0$ is the tensor formed from initial cell faces. In the Lagrangian, the Kohn-Sham energy $E(\mathbf{r}_i)$ and the applied pressure together correspond to the enthalpy, which plays the role of a generalized potential energy. Because the atomic positions in periclase are fixed by symmetry, the first term, which gives the kinetic energy associated with the ionic coordinates, is not required. The cubic structure of periclase further simplifies the Lagrangian: Only a single structural parameter, the cell parameter, needs to be determined for each pressure. For a given applied isotropic pressure, P, the lattice parameter converged when the total stress

$$\sigma_{ij} = \sigma_{ij}^c + \sigma_P - P \quad (i, j = 1, 2, 3) \quad (2)$$

was reduced to the order of 0.0001 eV/Å^3. In Equation 2, σ_{ij}^c is the self-consistent Hellman-Feynman stress tensor (Nielsen and Martin 1985), and σ_P is the isotropic Pulay stress (Francis and Payne 1990). The Pulay stress originates from the variation of the plane-wave basis set with lattice parameter. This correction is given by

$$\sigma_P = \frac{2}{3V} \frac{dE}{d \ln \epsilon_c} \quad (3)$$

where ϵ_c is the cutoff energy that limits the size of the

basis set to be used. As the unit cell changes size, the cutoff energy also changes because the k vector of the plane wave remains commensurate with the unit cell, and this, in turn, leads to a change in total energy (E). The Pulay stress was determined by calculating the total energy at several cutoffs and evaluating $dE/d \ln \epsilon_c$, which is -0.7332 eV, so that the Pulay correction to the stress at zero pressure is approximately -4 GPa. The total energies and stresses converged much faster when the finite basis-set corrections were included.

Elasticity

According to Hooke's law (Nye 1985), the stress (σ) and strain (ϵ) for small deformations to a crystal are linearly related by

$$\sigma_{ij} = c_{ijkl}\epsilon_{kl} \quad (i, j, k, l = 1, 2, 3) \tag{4}$$

where the fourth-rank tensor c_{ijkl} is the elastic constant tensor. Thus, the elastic constants can be determined directly from the computation of the stress generated by small strains (Wentzcovitch et al. 1995). The cubic crystal has three independent elastic constants, c_{11}, c_{12}, and c_{44} (in the Voigt notation). The strained lattice (lattice vectors $\boldsymbol{a}'$) used to determine the elastic constants is related to the unstrained lattice ($\boldsymbol{a}$) by $\boldsymbol{a}' = (I + \epsilon)\boldsymbol{a}$, where I is the identity matrix. The strain tensor is

$$\epsilon = \begin{pmatrix} e & e/2 & 0 \\ e/2 & 0 & 0 \\ 0 & 0 & 0 \end{pmatrix} \tag{5}$$

so that Hooke's law gives

$$\sigma_{xx} = c_{11}e,\ \sigma_{yy} = \sigma_{zz} = c_{12}e,\ \sigma_{yz} = c_{44}e, \text{ and}$$
$$\sigma_{zx} = \sigma_{xy} = 0. \tag{6}$$

For the lower symmetry of the strained lattice, the $4 \times 4 \times 4$ k-point mesh yielded 20 special k points. The ion positions are still fixed by the symmetry, so in the strained lattice only electrons should be relaxed. Thus, at a given pressure, we first obtained the equilibrium primitive cell of MgO by relaxing the cell parameter and then deformed the cell with the strain in Equation 5. We calculated the strain-induced stresses as discussed in the previous section and used Equation 6 to determine the values of c_{11}, c_{12}, and c_{44} for MgO.

The elastic constants completely specify the elastic properties and acoustic velocities of a single crystal. For the purpose of comparing with seismological data, it is interesting to compute the elastic properties of an isotropic polycrystalline aggregate. The bulk modulus of such an aggregate is well defined, whereas the shear modulus is inherently uncertain, depending in detail on the arrangement and shape of the constituent crystals (Watt et al. 1976). The bulk modulus is related to the elastic constants by

$$K = \tfrac{1}{3}(c_{11} + 2c_{12}). \tag{7}$$

In our static (athermal) calculations, the adiabatic and isothermal bulk moduli are identical and are both given by Equation 7. The isotropic shear modulus in the Hashin-Shtrikman averaging scheme (Hashin and Shtrikman 1962) is given by

$$G = \tfrac{1}{2}(G_U + G_L) \tag{8}$$

where the upper and lower bounds are, respectively,

$$G_U = c_{44} + 2\left[\frac{5}{c_s - c_{44}} + \frac{18(K + 2c_{44})}{5c_{44}(3K + 4c_{44})}\right] \tag{9}$$

and

$$G_L = c_s + 3\left[\frac{5}{c_{44} - c_s} + \frac{12(K + 2c_s)}{5c_s(3K + 4c_s)}\right] \tag{10}$$

where $c_s = (c_{11} - c_{12})/2$.

Results and discussion

Equation of state

We obtained equilibrium lattice parameters for MgO at different pressures up to 150 GPa. The pressure-volume results were fitted to the fourth-order Birch-Murnaghan equation of state (Birch 1986)

$$P = 3K_0 f(1 + 2f)^{5/2}(1 + a_1 f + a_2 f^2) \tag{11}$$

where

$$f = \frac{1}{2}\left[\left(\frac{V_0}{V}\right)^{2/3} - 1\right]$$

$$a_1 = \frac{3}{2}(K_0' - 4)$$

$$a_2 = \frac{3}{2}\left[K_0 K_0'' + K_0'(K_0' - 7) + \frac{143}{9}\right]$$

yielding the zero-pressure bulk modulus and its first and second pressure derivatives as follows: $K_0 = 159.7$ GPa, $K_0' = 4.26$, and $K_0'' = -0.026$ GPa^{-1}, which differ insignificantly from the parameters obtained from a third-order fit: $K_0 = 159.4$ GPa, $K_0' = 4.28$, and $K_0'' = -0.027$ GPa^{-1}. This implies that the fourth order term (coefficient a_2 in Eq. 11) is negligibly small. Our calculated values of the shear modulus were fitted to the appropriate fourth-order finite-strain expansion (Duffy and Ahrens 1992), yielding, for the shear modulus and its first and second pressure derivatives at zero pressure, $G_0 = 121.5$ GPa, $G_0' = 2.18$, and $G_0'' = -0.034$ GPa^{-1}. These values differ appreciably from those obtained from a third-order fit: $G_0 = 126.8$ GPa, $G_0' = 1.80$, and $G_0'' = -0.022$ GPa^{-1}, indicating that the finite-strain expansion converges much more slowly for the shear modulus than it does for the pressure. Our calculated values of zero-pressure bulk and shear moduli and their pressure derivatives compare favorably with experiments (Carter et al. 1971; Jackson and Niesler 1982; Duffy and Ahrens 1995; Chopelas 1996), as shown in Table 1. Older static compression experiments, which yielded relatively high values of the bulk modulus of periclase, about 180 GPa (Perez-Albuerne

TABLE 1. Zero-pressure lattice constant, bulk and shear moduli, and their pressure derivatives for the B1 phase of MgO in comparison with experimental and other theoretical results

	a_0 (Å)	K_0 (GPa)	K_0'	K_0'' (1/GPa)	G_0 (GPa)	G_0'	G_0'' (1/GPa)
			Theory				
This study	4.2506	159.7	4.26	−0.026	121.5	2.18	−0.034
Chang and Cohen (1984)	4.191	146					
Bukowinski (1985)	4.221	155	4.16	−0.030			
Mehl and Cohen (1988)	4.167	172	4.09				
Isaak et al. (1990)	4.191	181.9	4.12	−0.023			
			Experiment				
Fei (unpublished)	4.2112*	160.03	4.20				
Carter et al. (1971)		157	4.3				
Jackson and Niesler (1982)		162.5	4.13(9)	−0.058(66)**	130.9	2.53	−0.033
Duffy and Ahrens (1995)		162.5	4.09(9)	−0.019(4)	130.8	2.5(1)	−0.026(45)
Chopelas (1996)		162.0	4.08(9)	−0.036(16)	130.9	2.56(6)	−0.030(10)

* Wyckoff (1963).
** Corrected value (Isaak et al. 1990).

and Drickamer 1965; Weaver et al. 1971; Mao and Bell 1979), are now understood to have been significantly biased by the presence of nonhydrostatic stresses (Duffy et al. 1995). We reproduced both the zero-pressure lattice constant and bulk modulus very well in comparison with previous pseudopotential (Chang and Cohen 1984) and LAPW (Mehl and Cohen 1988) calculations (Table 1). The calculated lattice constant over the pressure range studied is within 1% of the experiments. We slightly overestimated the lattice constant, which we attributed to the pseudopotential approximation because the LDA is expected to underestimate slightly the lattice constant, as confirmed by the LAPW method (Mehl and Cohen 1988). The equation of state of MgO periclase is shown along with experimental results (Perez-Albuerne and Drickamer 1965; Weaver et al. 1971; Mao and Bell 1979; Duffy et al. 1995) in Figure 1.

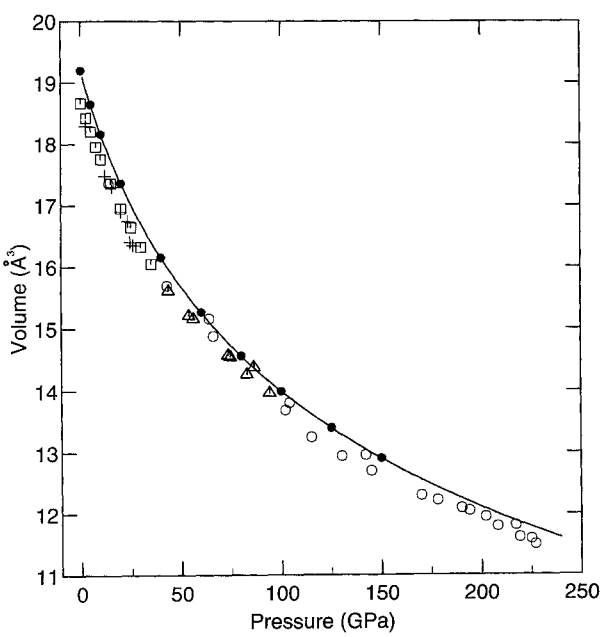

FIGURE 1. The equation of state for MgO. The solid curve represents the fourth-order Birch-Murnaghan fit to the calculated pressure-volume data (solid circles). The experimental data are from Perez-Albuerne and Drickamer (1965), Weaver et al. (1971), Mao and Bell (1979), and Duffy et al. (1995), shown by squares, plus signs, triangles, and open circles, respectively.

The B1-B2 phase transition

To investigate the B1-B2 phase transition in MgO, we calculated the enthalpy ($E + PV$) of the two-ion primitive cell of MgO in both the B1(NaCl) and B2(CsCl) structures as a function of pressure from 0 to 800 GPa (Fig. 2). The intersection of the two curves implies that the B1-B2 phase transition in MgO occurs at 451 GPa. By lowering the enthalpy of the B1 phase by 0.06 eV (the estimated uncertainty in the total energy), we obtained a transition pressure of 470 GPa. We expected the precision of the estimated phase transition to be much better than 20 GPa because the relative energies converge much faster than 0.06 eV. In agreement with previous calculations (Table 2), MgO is expected to transform from the B1 to the B2 phase at pressures much higher than other alkaline-earth oxides because of the small ratio of cation-to-anion radii. Our predicted value is much smaller than the previous pseudopotential value of 1050 GPa (Chang and Cohen 1984) and much larger than that predicted by some previous calculations (Cohen and Gordon 1976; Causà et al. 1986; Bukowinski 1985); however, it agrees closely with LAPW and PIB results (Mehl and Cohen 1988; Isaak et al. 1990; Zhang and Bukowinski 1991). No experimental evidence for the existence of the B1-B2 phase transition for MgO has been found up to 227 GPa from diamond-cell measurement (Duffy et al. 1995) and up to 200 GPa from shock-wave studies (Vassiliou and Ahrens 1981), demonstrating the remarkable stability range of MgO in the B1 phase. Thus, from both experimental and theoretical studies, the observed B1 structure for MgO seems to be stable throughout the Earth's mantle.

It is interesting to note the large discrepancy between the present result and the previous pseudopotential pre-

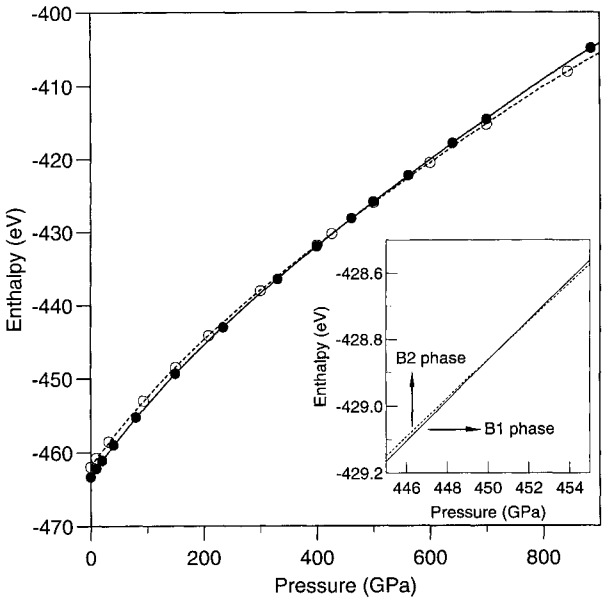

FIGURE 2. The B1-B2 phase transition in MgO. The solid line (solid circles) and dashed line (open circles) show the calculated zero-temperature free energies as a function of pressure for the NaCl and CsCl structures of MgO, respectively. The inset illustrates intersection of the curves, giving 451 GPa as the transition pressure.

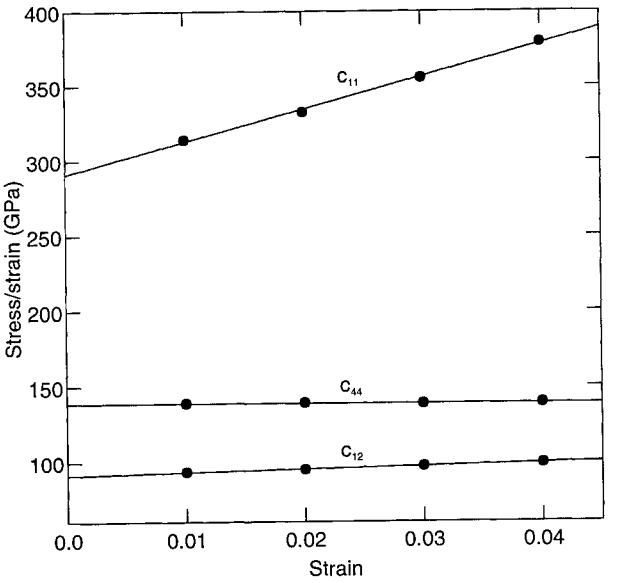

FIGURE 3. Stress/strain ratio vs. strain. The solid lines represent linear fits to the calculated values (solid circles) of stress/strain vs. strain for three elastic stiffness constants.

diction (Chang and Cohen 1984) for the transition pressure. We tested the transferability of our optimized pseudopotentials for both Mg and O. The size of the computational error (0.06 eV in energy) in our calculation is significantly smaller than that (0.5 eV) in the previous pseudopotential calculation. Furthermore, our prediction agrees very closely with the LAPW value, as mentioned above. Thus, we are confident in the reliability of our calculations. However, we are unable to use the pseudopotentials used by Chang and Cohen (1984) and are therefore unable to comment further on the observed disagreement between their results and ours.

Elastic moduli

We deformed the equilibrium primitive cell of MgO by using the strain defined in Equation 5 with different magnitudes: e = 0.01, 0.02, 0.03, and 0.04 (Mehl et al. 1990). We plotted the ratio of stress to strain vs. strain and determined c_{11}, for example, from the intercept of the best-fit line $\sigma_{xx}/e = c_{11} + O(e)$; and similarly for c_{12} and c_{44}. As shown in Figure 3, this procedure yielded c_{11} = 291, c_{12} = 91, and c_{44} = 139 GPa at zero pressure. We repeated this procedure at different pressures up to 150 GPa; the calculated values of c_{11}, c_{12}, and c_{44} are shown as a function of pressure in Table 3 and Figure 4. We used Equations 7–10 to calculate the isotropic aggregate bulk and shear moduli as a function of pressure as shown in Figure 4. The average of the Hashin-Shtrikman bounds agrees to within 1% of the Hill (1952) average, although the bounds on aggregate properties obtained by the Hashin-Shtrikman method are significantly narrower. The calculated zero-pressure values of all elastic moduli are slightly underestimated in comparison with the experimental values obtained from ultrasonic (Jackson and Niesler 1982) and resonance (Isaak et al. 1989) experiments (Table 4), consistent with slight overestimation of the calculated lattice constant (Table 1). Figure 4 shows the first- and second-order extrapolations of the low-pressure ultrasonic data of Jackson and Niesler (1982) to high pressure (up to 60 GPa) for all elastic moduli. The initial pressure dependence of the calculated elastic moduli agrees well with experiment, but at high pressures (beyond approximately 10 GPa) the calculated values differ substantially from the extrapolated data. Also, the second-order extrapolation deviates much more from the theoretical results at high pressure than does the corresponding linear extrapolation, as also noted by Isaak et al. (1990). This suggests that Taylor-series expansions of the pressure dependence of the elastic constants that use pres-

TABLE 2. Transition pressure, transition volume, and total-energy difference for the B1-B2 phase transition in MgO

	P_t (GPa)	V_t(B1) (Å^3)	V_t(B2) (Å^3)	ΔE (eV)
This study	451	9.887	9.429	1.273
Cohen and Gordon (1976)	256			
Chang and Cohen (1984)	1050	6.94	6.61	1.506
Bukowinski (1985)	205			
Causà et al. (1986)	220			
Mehl and Cohen (1988)	510	9.03	8.61	1.27
Isaak et al. (1990)	486			
Zhang and Bukowinski (1991)	580			

TABLE 3. Pressure variation of the lattice constant (Å), density (g/cm³), elastic moduli (GPa), and wave velocities (km/s) for MgO from 0 to 150 GPa

P	a	ρ	c_{11}	c_{12}	c_{44}	K	G_U	G_L	G	V_P	V_S
0	4.251	3.486	291	91	139	158	121.94	121.73	121.8	9.58	5.91
5	4.209	3.590	334	101	142	179	131.22	131.17	131.2	9.92	6.04
10	4.173	3.685	379	108	146	198	141.71	141.70	141.7	10.25	6.20
20	4.110	3.856	464	123	154	237	160.38	160.41	160.4	10.81	6.45
40	4.012	4.144	634	155	166	315	192.1	192.5	192.3	11.74	6.81
60	3.937	4.386	796	183	174	387	217.6	219.4	218.5	12.44	7.06
80	3.877	4.596	951	216	182	461	239.7	243.6	241.6	13.05	7.25
100	3.825	4.785	1112	246	186	535	258.2	265.5	261.9	13.59	7.40
125	3.780	4.998	1302	276	190	618	278.0	291.0	284.5	14.13	7.55
150	3.723	5.189	1497	299	194	698	297.3	317.4	307.3	14.61	7.69

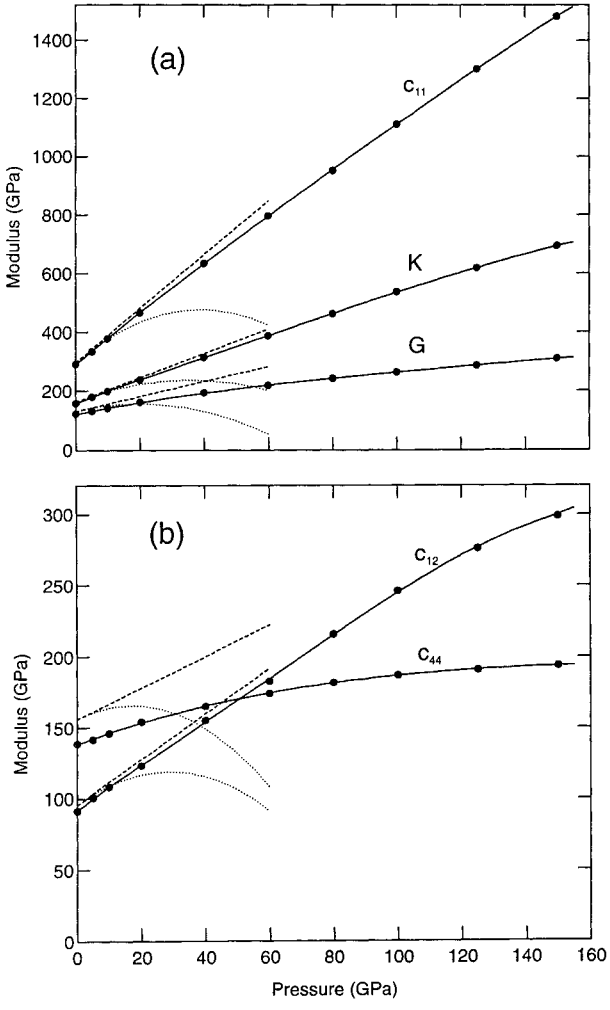

FIGURE 4. Pressure dependence of (**a**) c_{11}, K, and G, and (**b**) c_{12} and c_{44} of MgO. The symbols represent the calculated values, and the solid lines are the best fits. The first- and second-order extrapolations of low-pressure ultrasonic data (Jackson and Niesler 1982) to high pressure (up to 60 GPa) are shown by dashed and dotted lines, respectively.

sure as the expansion variable (rather than, for instance, finite strain) converge very slowly.

Isotropic wave velocities

We calculated the longitudinal and shear-wave velocities, V_P and V_S, respectively, of an isotropic aggregate using

$$V_P = \sqrt{\frac{K + \frac{4}{3}G}{\rho}} \quad \text{and} \quad V_S = \sqrt{\frac{G}{\rho}} \qquad (12)$$

where ρ is the density of the mineral. Like elastic moduli, the calculated density and wave velocities at zero pressure are also slightly underestimated with respect to experiments (Jackson and Niesler 1982; Isaak et al. 1989), as shown in Table 4. Figure 5 is a plot of V_P and V_S vs. pressure along with available experimental data (Jackson and Niesler 1982) and the seismically derived wave velocities in the lower mantle (Dziewonski and Anderson 1981). The high-pressure longitudinal and shear-wave velocities for MgO differ by <5% from the lower mantle seismic velocities. This small difference is somewhat coincidental for several reasons. First, the lower mantle is expected to be primarily composed of Mg-rich silicate perovskite with secondary magnesiowüstite. Second, magnesiowüstite is expected to contain several tens of percent FeO and to be subject to temperatures of 2000–3000 K. The effects of composition and temperature are expected to reduce the P- and S-wave velocities of magnesiowüstite relative to zero-temperature periclase by a few tens of percent.

TABLE 4. Zero-pressure athermal elastic moduli (GPa) and isotropic velocities (km/s)

	c_{11}	c_{12}	c_{44}	K	G	V_P	V_S
Calc.	291	91	139	158	122	9.58	5.91
Ult.*	296.8	95.3	155.8	162.5	130.8	9.71	6.05
Res.**	299	96.4	157.1	163.9	131.8	9.73	6.06

Note: The PIB values are $c_{11} - c_{12} = 188.5$ and $c_{44} = 187.6$ GPa (Isaak et al. 1990).

* Ultrasonic data (Jackson and Niesler 1982).

** Resonance data (Isaak et al. 1989).

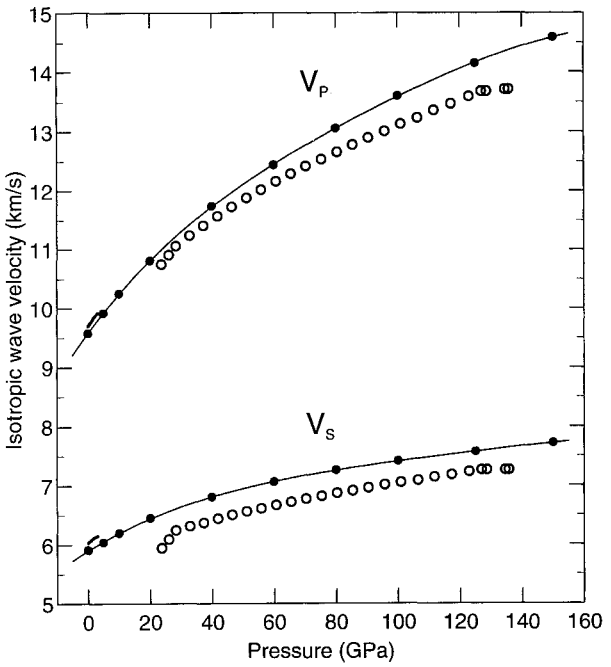

FIGURE 5. The isotropic longitudinal and shear-wave velocities, V_P and V_S, respectively, of MgO as a function of pressure. The calculated values (solid circles) are compared with the seismically derived velocities (open circles) of the lower mantle over the pressure regime of the lower mantle. The ultrasonic results up to 3 GPa from Jackson and Niesler (1982) are shown by thick solid lines.

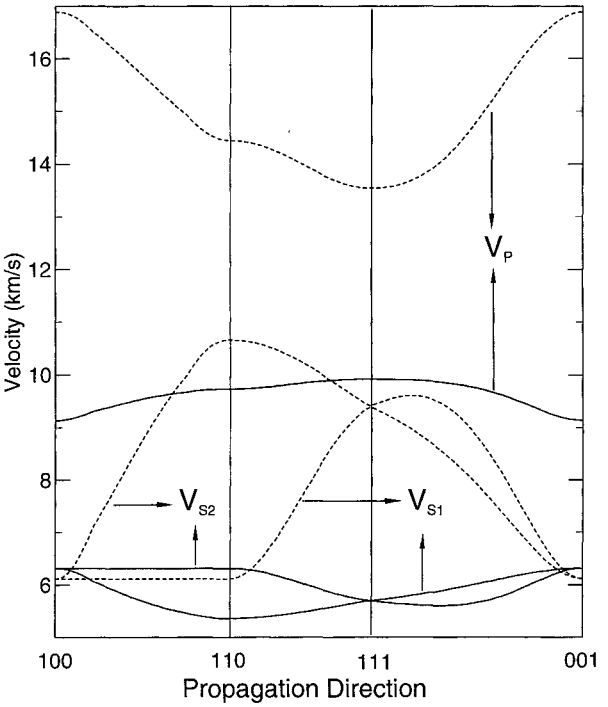

FIGURE 6. Dependence of the longitudinal (V_P) and two shear-wave velocities (V_{S1} and V_{S2}) of MgO on propagation direction at two pressures: the solid curves at 0 GPa and the dashed curves at 150 GPa.

Elastic anisotropy

The single-crystal elastic wave velocities in different directions are given by the Cristoffel equation

$$|c_{ijkl}n_jn_l - \rho V^2\delta_{ik}| = 0 \quad (13)$$

where c_{ijkl} is the single-crystal elastic constant tensor, $\boldsymbol{n}$ is the propagation direction, ρ is the density, V is the velocity, and δ_{ij} is the Kroenecker delta function. The eigenvalues of the 3×3 matrix yield the three unique elastic wave velocities for propagation direction $\boldsymbol{n}$, whereas the eigenvectors yield the polarization directions (Musgrave 1970). We found that MgO is highly anisotropic in both longitudinal and shear-wave velocities (Fig. 6). Longitudinal wave velocities are extremal for [100] and [111] propagation directions, whereas shear waves polarized in the $(\bar{1}10)$ plane (S1) are extremal along [100] and [110]. Velocities along these directions are shown in Table 5. In addition, shear waves polarized in the (001) plane (S2) show a local extremum in the shear velocity for propagation along $[\frac{1}{2},\frac{1}{2},1/\sqrt{2}]$.

A measure of the anisotropy of the elastic wave velocity in a cubic crystal is

TABLE 5. Pressure dependence of the longitudinal and two shear-wave velocities (km/s) in three directions from 0 to 150 GPa

	[100]			[110]			[111]				
P	V_P	V_{S1}	V_{S2}	V_P	V_{S1}	V_{S2}	V_P	V_{S1}	V_{S2}	Δ_P	Δ_S
0	9.14	6.31	6.31	9.73	5.36	6.31	9.92	5.69	5.69	8.1	16.2
5	9.65	6.29	6.29	10.01	5.70	6.29	10.12	5.90	5.90	4.7	9.8
10	10.14	6.30	6.30	10.28	6.01	6.30	10.33	6.14	6.14	1.9	4.7
20	10.97	6.32	6.32	10.77	6.32	6.65	10.71	6.54	6.54	2.4	5.1
40	12.37	6.33	6.33	11.63	6.33	7.60	11.37	7.20	7.20	8.5	18.7
60	13.47	6.30	6.30	12.30	6.30	8.36	11.88	7.74	7.74	12.8	29.2
80	14.39	6.29	6.29	12.91	6.29	8.94	12.37	8.15	8.15	15.5	36.6
100	15.24	6.23	6.23	13.44	6.23	9.51	12.79	8.56	8.56	18.0	44.3
125	16.14	6.16	6.16	14.00	6.16	10.13	13.20	9.00	9.00	20.8	52.6
150	16.89	6.11	6.11	14.45	6.11	10.67	13.54	9.40	9.40	23.0	59.3

Note: V_{S1} and V_{S2} are shear velocities that are respectively polarized in the $(\bar{1}10)$ and (001) planes along propagation direction [110]. $\Delta_P = [(V_{Pmax} - V_{Pmin})/V_{Pagg}]100$ and $\Delta_S = [(V_{Smax} - V_{Smin})/V_{Sagg}]100$.

$$A_X = \frac{M_X[\boldsymbol{n}_0] - M_X[100]}{c_{11}} \quad (14)$$

where $\boldsymbol{n}_0$ is the extremal propagation direction other than [100], X = P, S1, S2, and M_X is the modulus corresponding to the acoustic velocity, $M_X = \rho V_X^2$. One can show from the Cristoffel equation that for cubic crystals, A_X is related to the elastic anisotropy factor

$$A = \frac{2c_{44} + c_{12}}{c_{11}} - 1 \quad (15)$$

which is zero for an isotropic material. The anisotropies of P, S1, and S2 waves are then given by

$$A_P = \frac{2A}{3}, \quad A_{S1} = -\frac{A}{2}, \quad \text{and} \quad A_{S2} = -\frac{3A}{8}. \quad (16)$$

The pressure dependence of A is shown in Figure 7. The anisotropy factor drops rapidly with pressure initially, changes sign near 15 GPa, and then decreases more slowly at higher pressures. The nature of the anisotropy changes qualitatively near 15 GPa, as evidenced by the change of sign of A. Linear extrapolations of ultrasonic data and the PIB model have shown a similar change at 20 and 45 GPa, respectively (Duffy et al. 1995). The above relations (Eq. 16) explain the corresponding pressure-induced variations in the directions and polarizations of P and S waves with extremum velocities. At zero pressure, P waves are fastest along [111] (A positive) and S waves are slowest along [110], whereas at high pressure, P waves are fastest along [100] (A negative) and S waves are fastest along [110]. The pressure-induced change of sign of A also explains why S2 shear waves are fastest at low pressure and S1 shear waves are fastest at high pressure. The magnitudes of the P- and S-wave anisotropies also change substantially with pressure. The compressional and shear-wave velocities vary by 8 and 16%, respectively, at zero pressure and by 23 and 59%, respectively, at 150 GPa (Table 5).

The above results have potentially important implications for the interpretation of seismological observations of the anisotropy in terms of flow in the upper mantle (Tanimoto and Anderson 1984). To interpret the observations in terms of texturing induced by flow requires estimates of the elastic constants of major mantle minerals. These estimates are generally taken from zero-pressure experiments. Our results, however, suggest that elasticity at zero pressure may be a poor approximation of the elasticity even at relatively low pressures (10 GPa). We found that the anisotropy of periclase drops to nearly zero over the pressure range of the upper mantle (0–14 GPa) before increasing again at higher pressure. Periclase itself is not relevant for interpreting observations of upper mantle anisotropy. However, our results clearly show that anisotropy can be strongly pressure dependent, and that the anisotropy of minerals under mantle conditions may differ qualitatively from that at ambient conditions.

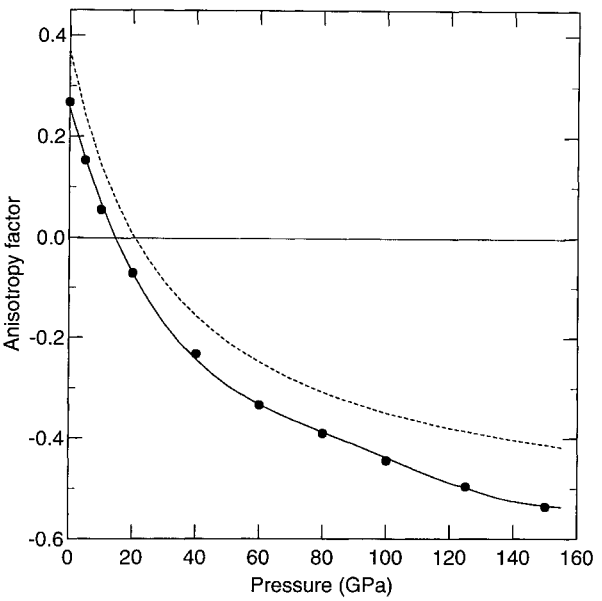

FIGURE 7. Pressure variation of the anisotropy factor, A, of MgO. The circles represent the calculated values. The first-order extrapolation from ultrasonic data (Jackson and Niesler 1982) is shown by the dashed line.

Cauchy relations

The Cauchy relation $c_{12} - c_{44} = 2P$ is valid only when all interatomic forces are central under static lattice conditions. At zero pressure, we found $c_{12} - c_{44} = -48$ GPa in comparison with the experimental value of -61 GPa (Jackson and Niesler 1982), indicating violation of the Cauchy condition in MgO. As pressure increases, the calculated value of $c_{12} - c_{44} - 2P$ decreases (greater Cauchy violation). The decrease is relatively slow up to 100 GPa and then rapid between 100 and 150 GPa, as shown in Figure 8. The relatively faster decrease above 100 GPa is due to the slow increase of c_{12} between 100 and 150 GPa. The initial pressure dependence of the deviation from the Cauchy condition agrees fairly well with low-pressure ultrasonic behavior (Fig. 8). The PIB model, with a zero-pressure value of -72 GPa for $c_{12} - c_{44} - 2P$, has shown a very similar pressure dependence of the Cauchy violation (Isaak et al. 1990).

The large violations of the Cauchy relation in MgO require an important contribution from noncentral forces. Periclase cannot be thought of as a material composed of rigid ions. Band-structure calculations indicate that periclase remains a wide-gap insulator to pressures well beyond those in the mantle, and that covalent bonding is not important (Bukowinski 1980), so metallic binding or covalent forces cannot explain the Cauchy violations. The prediction by PIB calculations of a Cauchy violation similar to our results indicates that this simplified model includes the essential physics. The relevant many-body force is a spherically symmetric breathing of the O ion

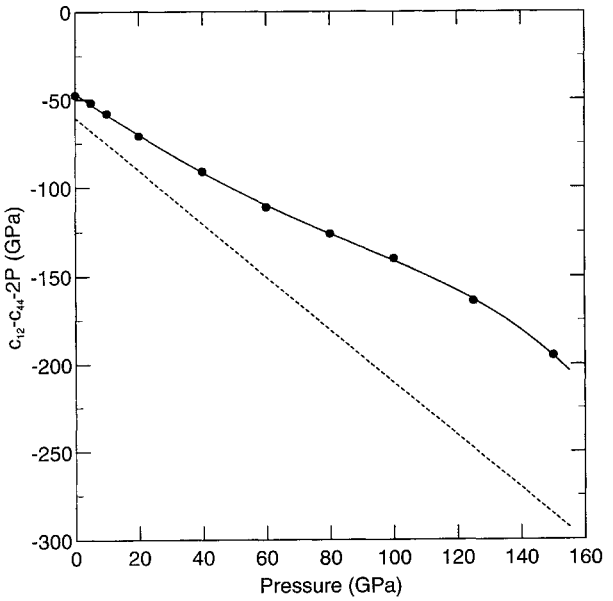

FIGURE 8. Pressure variation of the Cauchy violation in MgO. The circles represent the calculated values. The first-order extrapolation from ultrasonic data (Jackson and Niesler 1982) is shown by the dashed line.

in response to strain-induced variations in the Madelung potential at the O site.

ACKNOWLEDGMENTS

The authors thank EPSRC for computing facilities supported by grant GRIK74067, M.C. Payne for the original CASTEP code, and M.H. Lee for pseudopotentials. B.B.K. acknowledges support from the University of Edinburgh for granting the Premier Scholarship for postgraduate research and thanks H.C. Hsueh for useful discussions. L.S. was supported by the National Science Foundation under grant EAR-9305060. M.C.W. and S.J.C. thank the EPSRC for support. J.C. acknowledges support from the Royal Society of Edinburgh.

REFERENCES CITED

Anderson, O.L., and Andreatch, P., Jr. (1966) Pressure derivative of elastic constants of single crystal MgO at 23 and −195.8 °C. Journal of American Ceramic Society, 49, 404–409.

Birch, F.D. (1986) Equation of state and thermodynamic parameters of NaCl to 300 kbar in the high-temperature domain. Journal of Geophysical Research, 91, 4949–4954.

Bogardus, E.H. (1965) Third order elastic constants of Ge, MgO, and fused SiO_2. Journal of Applied Physics, 36, 2504–2513.

Bukowinski, M.S.T. (1980) Pressure effects on bonding in MgO. Journal of Geophysical Research, 85, 285–292.

——— (1985) First principles equations of state of MgO and CaO. Geophysical Research Letters, 12, 536–539.

Carter, W.J., Marsh, S.P., Fritz, J.N., and McQueen, R.G. (1971) The equation of state of selected materials for high-pressure reference. In Accurate Characterization of the High-Pressure Environment, NBS Special Publication, 326, 147–158.

Causà, M., Dovesi, R., Pisani, C., and Roetti, C. (1986) Electronic structure and stability of different crystal phases of magnesium oxide. Physical Review B, Condensed Matter, 33, 1308–1316.

Chang, K.J., and Cohen, M.L. (1984) High pressure behavior of MgO: Structural and electronic properties. Physical Review B, Condensed Matter, 30, 4774–4781.

Chang, Z.P., and Barsch, G.P. (1969) Pressure dependence of the elastic constants of single-crystalline magnesium oxide. Journal of Geophysical Research, 74, 3291–3294.

Chopelas, A. (1996) The fluorescence sideband method for obtaining acoustic velocities at high compressions: Application to MgO and $MgAl_2O_4$. Physics and Chemistry of Minerals, 23, 25–37.

Cohen, A.J., and Gordon, R.G. (1976) Modified electron-gas study of the stability, elastic properties, and high-pressure behavior MgO and CaO crystals. Physical Review B, Solid State, 14, 4593–4605.

Cohen, M.L., and Chelikowsky, J.R. (1988) Electronic structure and optical properties of semiconductors, 88 p. Springer-Verlag, New York.

Duffy, T.H., and Ahrens, T.J. (1992) Sound velocities at high pressure and temperature and their geophysical implications. Journal of Geophysical Research, 97, 4503–4520.

——— (1995) Compressional sound velocity, equation of state, and constitutive response of shock-compressed magnesium oxide. Journal of Geophysical Research, 100, 529–542.

Duffy, T.H., Hemley, R.J., and Mao, H.K. (1995) Equation of state and shear strength at multimegabar pressures: Magnesium oxide to 227 GPa. Physical Review Letters, 74, 1371–1374.

Dziewonski, A.M., and Anderson, O.L. (1981) Preliminary reference earth model. Physics of Earth and Planetary Interiors, 25, 297–356.

Francis, G.P., and Payne, M.C. (1990) Finite basis set corrections to total-energy pseudopotential calculations. Journal of Physics, Condensed Matter, 2, 4395–4404.

Hashin, Z., and Shtrikman, S. (1962) A variational approach to the theory of the elastic behavior of polycrystals. Journal of Mechanics and Physics of Solids, 10, 343–352.

Hill, R. (1952) The elastic behavior of a crystalline aggregate. Proceedings of the Physical Society London, 65A, 349–354.

Hsueh, H.C., Warren, M.C., Vass, H., Clark, S.J., Ackland, G.J., and Crain, J. (1996) Vibrational properties of the layered semiconductor germanium sulfide under pressure: Theory and experiments. Physical Review B, 53, 14806–14817.

Inbar, I., and Cohen, R.E. (1995) High pressure effects on thermal properties of MgO. Geophysical Research Letters, 22, 1193–1204.

Isaak, D.G., Anderson, O.L., and Goto, T. (1989) Measured elastic moduli of single crystal MgO up to 1800 K. Physics and Chemistry of Minerals, 16, 704–713.

Isaak, D.G., Cohen, R.E., and Mehl, M.E. (1990) Calculated elastic constants and thermal properties of MgO at high pressures and temperatures. Journal of Geophysical Research, 95, 7055–7067.

Jackson, I., and Niesler, H. (1982) The elasticity of periclase to 3 GPa and some geophysical implications. In S. Akimoto and M.H. Manghnani, Eds., High-pressure research in geophysics, p. 93–133. Center for Academic Publications, Tokyo.

Kleinman, L., and Bylander, D.M. (1982) Efficacious form for model pseudopotentials. Physical Review Letters, 48, 1425–1428.

Kohn, W., and Sham, L.J. (1965) Self-consistent equations including exchange and correlation effects. Physical Review, 140, A1133–A1138.

Lee, M.H. (1995) Advanced pseudopotentials for large scale electronic structure calculations. Ph.D. thesis, University of Cambridge, U.K.

Lin, J.S., Qteish, A., Payne, M.C., and Heine, V. (1993) Optimised and transferable non-local separable ab-initio pseudopotentials. Physical Review B, 47, 4174–4180.

Mao, H.K., and Bell, P.M. (1979) Equation of state of MgO and ϵ Fe under static pressure conditions. Journal of Geophysical Research, 84, 4533–4536.

Mehl, M.J., and Cohen, R.E. (1988) Linearized augmented plane wave electronic structure calculations for MgO and CaO. Journal of Geophysical Research, 93, 8009–8022.

Mehl, M.J., Osburn, J.E., Papaconstantopoulos, D.A., and Klein, B.M. (1990) Structural properties of ordered high-temperature intermetallic alloys from first-principles total-energy calculations. Physical Review B, Condensed Matter, 41, 10311–10323.

Monkhurst, H.J., and Pack, J.D. (1976) Special points for Brillouin-zone integrations. Physical Review B, Solid State, 13, 5188–5192.

Musgrave, M.J.P. (1970) Crystal acoustics: Introduction to the study of elastic waves and vibrations in crystals. In Holden-Day mathematical physics, 288 p. Holden-Day, San Francisco.

Nielsen, O.H., and Martin, R. (1985) Quantum mechanical theory of stress and force. Physical Review B, 32, 3780–3791.

Nye, J.F. (1985) Physical properties of crystals, 329 p. Clarendon, Oxford, U.K.

Payne, M.C., Teter, M.P., Allen, D.C., Arias, T.A., and Joannopoulos, J.D. (1992) Iterative minimisation techniques for ab initio total-energy calculations: Molecular dynamics and conjugate gradients. Reviews of Modern Physics, 64, 1045–1097.

Perdew, J., and Zunger, A. (1981) Self-interaction correction to density functional approximations for many-electron systems. Physical Review B, Condensed Matter, 23, 5048–5079.

Perez-Albuerne, E.A., and Drickamer, H.G. (1965) Effect of high pressures on the compressibilities of seven crystals having NaCl or CsCl structure. Journal of Chemical Physics, 43, 1381–1387.

Spetzler, H. (1970) Equation of state of polycrystalline and single crystal MgO to 8 kilobars and 800 K. Journal of Geophysical Research, 75, 2073–2087.

Tanimoto, T., and Anderson, D.L. (1984) Mapping convection in the mantle. Geophysical Research Letters, 11, 287–290.

Vassiliou, M.S., and Ahrens, J.J. (1981) Hugoniot equation of state of periclase to 200 GPa. Geophysical Research Letters, 8, 729–732.

Warren, M.C., and Ackland, G.J. (1996) Ab initio studies of structural instabilities in magnesium silicate perovskite. Physics and Chemistry of Minerals, 23, 107–118.

Watt, J.P., Davies, G.F., and O'Connell, R.J. (1976) The elastic properties of composite materials. Reviews of Geophysics and Space Physics, 14, 541–563.

Weaver, J.S., Takahashi, T., and Bassett, W.A. (1971) Calculation of the *P-V* relation for sodium chloride up to 300 kilobars at 25 °C. In E.C. Lloyd, Ed., Accurate characterization of the high-pressure environment, p. 189–199. NBS Special Publication 326.

Wentzcovitch, R.M. (1991) Invariant molecular dynamics approach to structural phase transitions. Physical Review B, 44, 2358–2361.

Wentzcovitch, R.M., Martins, J.L., and Price, G.D. (1993) Ab initio molecular dynamics with variable cell shape: Application to $MgSiO_3$ perovskite. Physical Review Letters, 70, 3947–3950.

Wentzcovitch, R.M., Ross, N.L., and Price, G.D. (1995) Ab initio study of $MgSiO_3$ and $CaSiO_3$ perovskites at lower mantle pressures. Physics of Earth and Planetary Interiors, 90, 101–112.

Wyckoff, R.W.G. (1963) Crystal structure, 88 p. Wiley, New York.

Zhang, H., and Bukowinski, M.S.T. (1991) Modified potential-induced-breathing model of potentials for close-shell ions. Physical Review B, 44, 2495–2503.

Manuscript received February 23, 1996
Manuscript accepted October 1, 1996